AIAA 92-0694

Solidification of Variable Property Melts Under the Influence of Low Gravity, Magnetic Fields and Electric Fields

G.S. Dulikravich and B. Kosovic
Department of Aerospace Engineering
Penn State University
University Park, PA 16802

30th Aerospace Sciences Meeting & Exhibit
January 6-9, 1992 / Reno, NV

SOLIDIFICATION OF VARIABLE PROPERTY MELTS UNDER THE INFLUENCE OF LOW GRAVITY, MAGNETIC FIELDS AND ELECTRIC FIELDS

George S. Dulikravich[1] and Branko Kosovic[2]
Department of Aerospace Engineering, 233 Hammond Building
The Pennsylvania State University, University Park, PA 16802, USA

ABSTRACT

Systems of partial differential equations governing three-dimensional laminar flow of an incompressible viscous fluid undergoing solidification under the influence of externally applied gravitational, magnetic and electric fields have been formulated. The model uses an extended Boussinesq approximation to allow for temperature dependent physical properties. It includes effects of Joule heating, latent heat release, Lorentz force and ponderomotive force. The system of coupled partial differential equations was solved using an artificial compressibility formulation and explicit finite differencing with a four-step Runge-Kutta time integration. Preliminary two-dimensional numerical results demonstrate the ability of the externally applied magnetic and electric fields to influence the melt recirculation, the amount of solid phase accrued, and the solid/liquid interface shape.

NOMENCLATURE

$\tilde{\mathbf{A}}$ = ξ-flux vector Jacobian in curvilinear nonorthogonal coordinates

b = charged particles mobility coefficient [$m^2\ s^{-1}\ V^{-1}$]

$\tilde{\mathbf{B}}$ = η-flux vector Jacobian in curvilinear nonorthogonal coordinates

c_P = specific heat coefficient [$m^2\ K^{-1}\ s^{-2}$]

$\tilde{\mathbf{C}}$ = ζ-flux vector Jacobian in curvilinear nonorthogonal coordinates

D = diffusivity of charged particles [$m^2\ s^{-1}$]

D = differential operator

$\mathbf{D}$ = diagonal matrix

$\boldsymbol{E}$ = electric field vector [$V\ m^{-1}$]

E_x, E_y, E_z = x, y and z component of the electric field vector

$\tilde{\mathbf{E}}$ = ξ-flux vector in curvilinear nonorthogonal coordinates

$\tilde{\mathbf{F}}$ = η-flux vector in curvilinear nonorthogonal coordinates

g_{ij} = metric tensor

$\mathbf{g}$ = gravity force per unit volume [$N\ m^{-3}$]

$\tilde{\mathbf{G}}$ = ζ-flux vector in curvilinear coordinates

$\mathbf{H}$ = magnetic field [$H\ kg^{-1}$]

$\mathbf{I}$ = identity matrix

$\mathbf{J}$ = electric current per unit volume [$A\ m^{-3}$]

k = heat conductivity coefficient [$kg\ m\ s^{-3}\ K^{-1}$]

k_b = Boltzman's constant [$kg^{-1}\ s\ K$]

l = length [m]

L = latent heat of liquid/solid phase change [$J\ kg^{-1}$]

$\mathbf{n}$ = unit vector normal to the solid wall

p = pressure [$N\ m^{-2}$]

$\bar{p}$ = combined pressure [$N\ m^{-2}$]

q = electric charge density per unit volume [$kg\ m^{-1}\ s^{-2}\ V^{-1}$]

$\tilde{\mathbf{Q}}$ = solution vector in curvilinear nonorthogonal coordinates

$\tilde{\mathbf{R}}$ = residual vector

S = volume fraction of the liquid phase

$\tilde{\mathbf{S}}$ = source term vector in curvilinear nonorthogonal coordinates

t = time [s]

T = temperature [K]

---

[1]Associate Professor. Associate Fellow AIAA.

[2]Graduate Student. Student Member AIAA.

ΔT = temperature difference [K]
u, v, w = velocity components in Cartesian coordinates [m s^{-1}]
U, V, W = contravariant velocity components [m s^{-1}]
v = velocity vector in Cartesian coordinates [m s^{-1}]
x,y,z = Cartesian coordinates [m]
α = thermal expansion coefficient [K^{-1}]
β = artificial compressibility coefficient
δ = smoothing operator
ε = electrical permitivity coefficient [kg m s^{-2} V^{-2}]
ε_4 = fourth order artificial dissipation coefficient
ξ,η,ζ = curvilinear coordinates [m]
η = viscosity coefficient [kg m^{-1} s^{-1}]
ω = smoothing coefficient for residual
ϕ = non-dimensional gravity potential
φ = electric potential [V]
ψ = artificial dissipation sensor function
ρ = fluid density [kg m^{-3}]
θ = nondimensional temperature difference
ϕ = non-dimensional gravity potential
μ = magnetic permeability [H m^{-1}]
σ = electrical conductivity [Ω^{-1} m^{-1}]
Φ = viscous dissipation function [kg m^{-1} s^{-3}]

subscripts

c = cold wall
e = electrical
h = hot wall
o = reference values
E = electric

superscripts

* = nondimensional values
T = transpose of a matrix
' = function of nondimensional temp.

1. INTRODUCTION

During the solidification of melts significant residual stresses and nonuniform distribution of impurities regularly occur in the solidified material. During the cooling or thawing processes, secondary flows are generated due to strong buoyancy forces. These processes cannot be effectively controlled, except if influenced by a global body force. One such body force is the general electromagnetic Lorentz force which is created in any electrically conducting moving fluid when either a magnetic field or an electric potential field is applied. It has been well known that the magnetic field can eliminate vorticity from the flow field, while the electric field can enhance it so that the freezing front could be manipulated.

Stuetzer[1] was the first who clearly defined two extreme models for a fluid flow under the influence of electromagnetic fields: magnetohydrodynamics (MHD) and electrohydrodynamics (EHD)[2-6]. The MHD model assumes that there are no electrically charged particles in the flow field and that there is no electric potential applied[7-11]. EHD assumes that there is no magnetic field applied[12-16] while an external electric field is applied to an electrically conducting fluid containing electrically charged particles. In the EHD flows, the electrically charged particles are convected with the flow, they can diffuse and move under the influence of the outside (imposed) and inside (self-induced) electric field. When modeling EHD flows we must incorporate an equation for electric charge density preservation for each of the electrically charged species[4]. One equation governing the electric potential field must also be added. In the momentum equation an electrical (Lorentz) body force must be added. In the energy equation we must add a Joule heating term. In the case of solidification (phase change) a latent heat term must be added to the energy equation. Only incomplete versions of the EHD models have been numerically solved in the past. Our recent efforts[15-16] were among the first attempts at a consistent and complete modeling of the EHD flows. Nevertheless, to the best of our knowledge, the EHD flows that involve solidification have not been computed before.

The objective of this paper is to present a fully three-dimensional mathematical model in the Cartesian (physical) space and in the nonorthogonal curvilinear boundary-conforming (computational) space. Difficulties with the numerical algorithm for its solution will be discussed and very preliminary computational results for cases of two-dimensional steady laminar MHD and EHD flows involving solidification will be presented for the cases with full gravity and a reduced gravity.

2. MHD SOLIDIFICATION MODEL

2.1 General Definitions

The entire set of partial differential equations can be non-dimensionalized by introducing the relations

$$v^* = \frac{v}{v_o} \qquad x^* = \frac{x}{x_o} \qquad t^* = \frac{t\, v_o}{l_o}$$

$$p^* = \frac{p}{\rho_o\, v_o^2} \qquad g^* = \frac{g_i}{g} \qquad \Phi^* = \frac{\Phi}{\eta_o\, v_o^2/l_o^2}$$

$$H_i{}^* = \frac{H_i}{H_o} \qquad \theta = \frac{\Delta T}{\Delta T_o} \qquad e^* = \frac{e}{c_{po}\, \Delta T_o} \qquad (1)$$

Here, T_c is the temperature of the cold wall and T_h is the temperature of the hot wall, so that $\Delta T = T - T_c$ and $\Delta T_o = T_h - T_c$. With the following non-dimensional groups

Reynolds number $\quad Re = \dfrac{\rho_o\, v_o\, l_o}{\eta_o}$

Froude number $\quad Fr^2 = \dfrac{v_o^2}{g_o\, l_o}$

Prandtl number $\quad Pr = \dfrac{c_{po}\, \eta_o}{k_o}$

Grashof number $\quad Gr = \dfrac{\rho_o^2\, g_o\, \alpha_o\, \Delta T_o\, l_o^3}{\eta_o^2}$

Eckert number $\quad Ec = \dfrac{v_o^2}{c_{po}\, \Delta T_o}$

Prandtl number $\quad Pr = \dfrac{\eta_o\, c_{po}}{k_o}$

Magnetic Prandtl number $\quad Pm = \dfrac{\mu\, \sigma\, \eta_o}{\rho_o}$

Hartmann number $\quad Ht = \mu\, l_o\, H_o \left(\dfrac{\sigma}{\eta_o}\right)^{1/2}$

Magnetic Reynolds number $\quad Rm = Re\, Pm$

Magnetic Mach number $\quad Mm^2 = \dfrac{ReRm}{Ht^2} = \dfrac{\rho_o\, v_o^2}{\mu\, H_o^2}$ $\qquad (2)$

The non-dimensional density ρ' can be expanded in a Taylor series while retaining only the first order term, that is,

$$\rho' = 1 - \alpha\, \Delta T = 1 - \alpha^*\, \theta \qquad (3)$$

where

$$\alpha^* = \frac{\partial \rho'}{\partial \theta} = \frac{\Delta T_o\, \rho_o}{\rho_o\, \Delta T_o} \frac{\partial \rho'}{\partial \theta} = \frac{\Delta T_o}{\rho_o} \frac{\partial \rho}{\partial T} = \Delta T_o\, \alpha \qquad (4)$$

It can be assumed that the coefficient of thermal expansion, α, is constant in the range of temperatures which are of interest in a particular case. When the term $(\Delta T_o\, \alpha) \ll 1$, an extended form of the Boussinesq approximation can be derived for the fluid with non-constant physical properties[17].

2.2 Latent Heat Release Model

In the case of a liquid/solid mixture the enthalpy per unit mass of the mushy region becomes

$$dh = c_p\, dT + L\, dS \qquad (5)$$

where L is the latent heat (enthalpy of solid/liquid phase change) and S is the volumetric fraction of the solid phase. Then

$$v_i\, h_{,i} = c_p\, v_i\, T_{,i} - L\, v_i\, S_{,i} = \left(c_p - L\, S_{,T}\right)\, v_i\, T_{,i} \qquad (6)$$

Let $c_{pe} = c_p - L\, S_{,T}$ be an equivalent specific heat.

$$c_{pe} = c_{po}\, c_{pe}' = c_{po} \left(c_p' - \frac{L\, S_{,\theta}\, \theta_{,T}}{c_{po}}\right) \qquad (7)$$

Here, S could be an arbitrary function of θ and c_{pe}' is the non-dimensional equivalent specific heat. This approach is called the "enthalpy method"[18].

2.3 MHD Model

The non-dimensional MHD equations including solidification can finally be written as
Mass conservation:

$$v_{i,i} = 0 \tag{8}$$

Momentum conservation

$$v_{i,t} + \left(v_i\, v_j\right)_{,j} = \frac{1}{Re}\left(\eta'\, v_{i,j}\right)_{,j} - p_{,i} + \frac{Gr\,\theta}{Re^2}\, g_i + \frac{Ht^2}{RmRe}\left(H_i\, H_k\right)_{,k} \tag{9}$$

Energy conservation

$$\theta_{,t} + v_i\,\theta_{,i} = \frac{1}{RePr\, c_{pe}'}\left(k'\,\theta_{,i}\right)_{,i} + \frac{EcHt^2}{Rm^2Re\, c_{pe}'}\,\varepsilon_{ijk}\varepsilon_{ilm}H_{k,j}H_{m,l} \tag{10}$$

Magnetic field transport

$$H_{,t} - \left(v_j\, H_i - v_i\, H_j\right)_{,j} = \frac{1}{Rm}\, H_{i,jj} \tag{11}$$

where $\frac{1}{Mm^2}\varepsilon_{ijk}\,\varepsilon_{jlm}H_{m,l}H_k$ is ponderomotive force while $\frac{Ec}{Mm^2\, Rm}\,\varepsilon_{ijk}\varepsilon_{ilm}H_{k,j}H_{m,l}$ is Joule heating due to applied magnetic field and $\Phi^{(i)}$ is the energy dissipation function for incompressible viscous flow.

$$\Phi^{(i)} = \eta'\left(v_{i,j} + v_{j,i}\right) v_{i,j} \tag{12}$$

It should be pointed out that the viscous dissipation $\Phi^{(i)}$ can be neglected from an order of magnitude analysis. For example, for water with c_{po} = 4179 J/(kg K), ρ_0 = 1003 kg/m^3, η_0 = 0.0017 kg/(m s) it follows that

$$\frac{\rho_o\, c_{pe}\,\frac{\partial T}{\partial t}}{\Phi^{(i)}} = \frac{Re}{Ec} \approx 2.46 \times 10^9\,\frac{\Delta T_o\, l_o}{v_o} \tag{13}$$

The combination of non-dimensional hydrostatic, hydrodynamic, and magnetic pressures is

$$\bar{p} = p + \frac{\phi}{Fr^2} + \frac{1}{Mm^2}H_iH_i \tag{14}$$

where ϕ is the non-dimensional gravity potential defined as $g_i = \phi_{,i}$.

2.4 Numerical Algorithm for MHD

Equations (8-11) represent a global system of coupled non-linear partial differential equations. The global system has been split in two subsystems in order to simplify programming. The Navier-Stokes equations (8-10) constitute the first subsystem and magnetic field transport equations (11) constitute the second subsystem. To integrate each subsystem, the explicit Runge-Kutta time stepping method[19] was used in an alternating manner[7].

The general form of each subsystem is the same. When expressed in a fully conservative form in generalized curvilinear non-orthogonal coordinates they are

$$\frac{\partial \tilde{\mathbf{Q}}}{\partial t} + \frac{\partial \tilde{\mathbf{E}}}{\partial \xi} + \frac{\partial \tilde{\mathbf{F}}}{\partial \eta} + \frac{\partial \tilde{\mathbf{G}}}{\partial \zeta} = D^2 + \tilde{\mathbf{S}} \tag{15}$$

where $\tilde{\mathbf{Q}}$ is the solution vector and $\tilde{\mathbf{E}}$, $\tilde{\mathbf{F}}$ and $\tilde{\mathbf{G}}$ are the flux vectors. The transformed source vector is denoted by $\tilde{\mathbf{S}}$. For the Navier-Stokes equations, the generalized vectors are defined as

$$\tilde{\mathbf{Q}} = \frac{1}{J}\begin{bmatrix} \bar{p}/\beta \\ u \\ v \\ w \\ \theta \end{bmatrix} \qquad \tilde{\mathbf{E}} = \frac{1}{J}\begin{bmatrix} U \\ Uu + \xi_x\bar{p} \\ Uv + \xi_y\bar{p} \\ Uw + \xi_z\bar{p} \\ U\theta \end{bmatrix}$$

$$\tilde{\mathbf{F}} = \frac{1}{J}\begin{bmatrix} V \\ Vu + \eta_x\bar{p} \\ Vv + \eta_y\bar{p} \\ Vw + \eta_z\bar{p} \\ V\theta \end{bmatrix} \qquad \tilde{\mathbf{G}} = \frac{1}{J}\begin{bmatrix} W \\ Wu + \zeta_x\bar{p} \\ Wv + \zeta_y\bar{p} \\ Ww + \zeta_z\bar{p} \\ W\theta \end{bmatrix}$$

$$\tilde{\mathbf{S}} = \begin{bmatrix} 0 \\ \tilde{d}_2 \\ \tilde{d}_3 \\ \tilde{d}_4 \\ \tilde{d}_5 \end{bmatrix} \qquad \tilde{\mathbf{D}} = \frac{1}{Re}\begin{bmatrix} 0 \\ \eta' \\ \eta' \\ \eta' \\ \frac{k'}{Pr\, c_{pe}'} \end{bmatrix}^T \tag{16}$$

where $J = \frac{\partial(\xi,\eta,\zeta)}{\partial(x,y,z)}$ is the Jacobian determinant of the geometric transformation from physical Cartesian coordinates x, y, z into ξ, η, ζ computational space.

The system of equations given by (7-11) is not hyperbolic since there is no physical time derivative term in the mass conservation equation. Consequently, to integrate the system simultaneously and obtain a steady state solution, an artificial compressibility[20] term, $\frac{\partial}{\partial t}\left(\frac{\bar{p}}{\beta J}\right)$, has been added to the mass conservation equation. Here, β is an artificial compressibility coefficient, a user specified parameter that depends on the problem geometry, grid, flow parameters, etc.[21] In the steady state limit the artificial compressibility term tends to zero.

The source vector $\tilde{S}$ contains the influence of the ponderomotive force due to the magnetic field and the thermal buoyancy force. Its components are given as

$$\tilde{d}_2 = \frac{Ht^2}{RmRe}\left[\frac{\partial}{\partial\xi}\left(\frac{\hat{H}_\xi H_x}{J}\right) + \frac{\partial}{\partial\eta}\left(\frac{\hat{H}_\eta H_y}{J}\right) + \frac{\partial}{\partial\zeta}\left(\frac{\hat{H}_\zeta H_z}{J}\right)\right] + \frac{Gr\theta}{Re^2 J} e_\xi$$

$$\tilde{d}_3 = \frac{Ht^2}{RmRe}\left[\frac{\partial}{\partial\xi}\left(\frac{\hat{H}_\xi H_y}{J}\right) + \frac{\partial}{\partial\eta}\left(\frac{\hat{H}_\eta H_y}{J}\right) + \frac{\partial}{\partial\zeta}\left(\frac{\hat{H}_\zeta H_y}{J}\right)\right] + \frac{Gr\theta}{Re^2 J} e_\eta$$

$$\tilde{d}_4 = \frac{Ht^2}{RmRe}\left[\frac{\partial}{\partial\xi}\left(\frac{\hat{H}_\xi H_z}{J}\right) + \frac{\partial}{\partial\eta}\left(\frac{\hat{H}_\eta H_z}{J}\right) + \frac{\partial}{\partial\zeta}\left(\frac{\hat{H}_\zeta H_z}{J}\right)\right] + \frac{Gr\theta}{Re^2 J} e_\zeta$$

$$\tilde{d}_5 = \frac{1}{c_{pe}'}\frac{EcHt^2 J}{RmRe^2}\left[\tilde{P}_1^2 + \tilde{P}_2^2 + \tilde{P}_3^2\right] \qquad (17)$$

where H_x, H_y, H_z are the components of the magnetic field vector in Cartesian coordinates, e_ξ e_η, e_ζ are components of the unit vector in the direction of gravity force, and

$$\tilde{P}_1 = \frac{\partial}{\partial\xi}\left(\frac{H_z\xi_y - H_y\xi_z}{J}\right) + \frac{\partial}{\partial\eta}\left(\frac{H_z\eta_y - H_y\eta_z}{J}\right) + \frac{\partial}{\partial\zeta}\left(\frac{H_z\zeta_y - H_y\zeta_z}{J}\right)$$

$$\tilde{P}_2 = \frac{\partial}{\partial\xi}\left(\frac{H_x\xi_z - H_z\xi_x}{J}\right) + \frac{\partial}{\partial\eta}\left(\frac{H_x\eta_z - H_z\eta_x}{J}\right) + \frac{\partial}{\partial\zeta}\left(\frac{H_x\zeta_z - H_z\zeta_x}{J}\right)$$

$$\tilde{P}_3 = \frac{\partial}{\partial\xi}\left(\frac{H_y\xi_x - H_x\xi_y}{J}\right) + \frac{\partial}{\partial\eta}\left(\frac{H_y\eta_x - H_x\eta_y}{J}\right) + \frac{\partial}{\partial\zeta}\left(\frac{H_y\zeta_x - H_x\zeta_y}{J}\right) \qquad (18)$$

The diffusion term in general curvilinear coordinates is

$$D^2 = \left(\frac{\tilde{D}}{J} g_{ij}\left(J\tilde{Q}\right)_{,j}\right)_{,i} \qquad (19)$$

where g_{ij} is metric tensor. The contravariant components of velocity vector are denoted by U, V, W, while contravariant components of the magnetic field vector are $\hat{H}_\xi$, $\hat{H}_\eta$, $\hat{H}_\zeta$.

For the subsystem containing the magnetic field transport equations, the solution vector $\tilde{Q}$, the flux vectors $\tilde{E}$, $\tilde{F}$, $\tilde{G}$, and the source vector $\tilde{S}$ are

$$\tilde{Q} = \frac{1}{J}\begin{bmatrix} H_x \\ H_y \\ H_z \end{bmatrix} \quad \tilde{E} = \frac{1}{J}\begin{bmatrix} H_xU - u\hat{H}_\xi \\ H_yU - v\hat{H}_\xi \\ H_zU - w\hat{H}_\xi \end{bmatrix} \quad \tilde{F} = \frac{1}{J}\begin{bmatrix} H_xV - u\hat{H}_\eta \\ H_yV - v\hat{H}_\eta \\ H_zV - w\hat{H}_\eta \end{bmatrix}$$

$$\tilde{G} = \frac{1}{J}\begin{bmatrix} H_xW - u\hat{H}_\zeta \\ H_yW - v\hat{H}_\zeta \\ H_zW - w\hat{H}_\zeta \end{bmatrix} \quad \tilde{S} = 0 \quad \tilde{D} = \frac{1}{Rm} I \qquad (20)$$

Thus, in the case of three-dimensional magneto-hydrodynamics, the system of eight partial differential equations needs to be solved by integrating intermittently a subsystem of five fluid flow equations and a subsystem of three magnetic field transport equations and transferring the information through the source-like terms[7].

3. EHD Solidification Model

The system of EHD governing equations[1,15-16] is derived from a combination of Maxwell's equations of electrodynamics and the Navier-Stokes equations.

An idealized charged fluid is assumed and therefore magnetic fields can be neglected so that Maxwell's equations reduce to a charge conservation equation and Poisson's equation for electric potential. The electric permitivity ε is assumed to be uniform. Thus, the EHD governing equations are:

Mass conservation

$$\nabla \cdot v = 0 \tag{21}$$

Momentum (including thermal buoyancy force and electric Lorentz force)

$$\rho_o \frac{Dv}{Dt} = -\nabla p - \rho_o \alpha g \Delta T + \nabla \cdot (\eta_o \nabla v) + q E \tag{22}$$

Energy (including Joule heating)

$$\rho c_p \frac{DT}{Dt} = \nabla \cdot (k \nabla T) + J \cdot E \tag{23}$$

Electric charge conservation

$$\frac{\partial q}{\partial t} + \nabla \cdot J = 0 \tag{24}$$

Electric potential field

$$\nabla \cdot E = \frac{q}{\varepsilon} \tag{25}$$

The induced electric current per unit volume is given by Ohm's law

$$J = q (v + b E) - D \nabla q \tag{26}$$

The electric charge diffusivity coefficient D and mobility coefficient b are related by the Einstein's formula[7]

$$D = \frac{k_b T}{q m_i} \rho_i b \tag{27}$$

where m_i is the mass of a charged particle and ρ_i is the density of the electrically non-neutral fluid. Since

$$\nabla \times E = 0 \tag{28}$$

it follows that

$$E = -\nabla \varphi \tag{29}$$

where φ is the electric potential, so that equation (25) becomes

$$\nabla^2 \varphi = -\frac{q}{\varepsilon} \tag{30}$$

Nondimensionalization can be performed with respect to the reference values denoted by subscript o, so that

$$p^* = \frac{p}{\rho_o v_o^2} \qquad \varphi^* = \frac{\Delta\varphi}{\Delta\varphi_o} \qquad E^* = \frac{E l_o}{\Delta\varphi_o}$$

$$q^* = \frac{q}{q_o} \qquad b = b_o b'(\theta) \qquad g^* = \frac{g}{g_o} \tag{31}$$

Here, $\Delta\varphi_o$ is the reference value of the difference of the electric potential between the two walls. The following nondimensional groups should be recognized as

Charge diffusivity number $\quad D_E = \dfrac{\eta_o}{\rho_o D_o}$

Lorentz force number $\quad S_E = \dfrac{q_o \Delta\varphi_o}{\rho_o v_o^2}$

Electric Prandtl number $\quad Pr_e = \dfrac{\eta_o}{\rho_o b_o \Delta\varphi_o}$

Electric field number $\quad N_E = \dfrac{q_o l_o^2}{\varepsilon_o \Delta\varphi_o}$ (32)

Thus, the system of equations for incompressible flow of a fluid with temperature dependent properties and electric charges under the influence of an externally applied electric field reduces[15] to

$$\nabla^* \cdot v^* = 0 \tag{33}$$

$$\frac{\partial v^*}{\partial t^*} + \nabla^* \cdot (v^* v^* + p^* I) = \frac{1}{Re} \nabla^* \cdot (\eta' \nabla^* v^*) + \frac{Gr\,\theta}{Re^2} g^* + S_E q^* E^* \tag{34}$$

$$\frac{\partial \theta}{\partial t^*} + \nabla^*\cdot(\theta^* v^*) = \frac{1}{Pr\ Re\ c_{pe}'} \nabla^*\cdot (k' \nabla^* \theta) + \frac{S_E\ Ec}{c_{pe}'}(q^* (v^* + \frac{1}{Re\ Pr_E} E^*) - \frac{1}{Re\ D_E} \nabla^* q^*).E^* \quad (35)$$

$$\frac{\partial q^*}{\partial t^*} + \nabla^*\cdot\left[q^* (v^* + \frac{1}{Re\ Pr_E} E^*)\right] = + \frac{1}{Re} \nabla^*\cdot (\frac{1}{D_E} b'\nabla^* q^*) \quad (36)$$

$$\nabla^* 2\, \varphi^* = - N_E\, q^* \quad (37)$$

where $\tilde{p}^* = p^* + \frac{\phi^*}{Fr2}$ so that $g^* = \nabla^* \phi^*$.

3.2 EHD Numerical model

For simplicity and clarity of notation, the asterisk symbol in the system of equations (33-37) will be omitted.The electric potential field equation (37) is solved separately. After transformation to generalized curvilinear non-orthogonal boundary-conforming coordinates in computational space, the system of governing equations can be written as

$$\frac{\partial \vec{Q}}{\partial t} + \frac{\partial \vec{E}}{\partial \xi} + \frac{\partial \vec{F}}{\partial \eta} + \frac{\partial \vec{G}}{\partial \zeta} = D\ 2(J\vec{Q}) + \vec{S} \quad (38)$$

The solution vector, flux and source term vectors in curvilinear coordinates are

$$\vec{Q}=\frac{1}{J}\begin{bmatrix} \tilde{p}/\beta \\ u \\ v \\ w \\ \theta \\ q \end{bmatrix} \qquad \vec{E}=\frac{1}{J}\begin{bmatrix} U \\ Uu+\xi_x\tilde{p} \\ Uv \\ Uw \\ U\theta \\ q(U+\frac{1}{RePr_E} E_\xi) \end{bmatrix}$$

$$\vec{F}=\frac{1}{J}\begin{bmatrix} V \\ Vu \\ Vv+\eta_y\tilde{p} \\ Vw \\ V\theta \\ q(V+\frac{1}{RePr_E} E_\eta) \end{bmatrix} \quad (39)$$

$$\vec{G}=\frac{1}{J}\begin{bmatrix} W \\ Wu \\ Wv \\ Ww+\zeta_z\tilde{p} \\ W\theta \\ q(W+\frac{1}{RePr_E} E_\zeta) \end{bmatrix} \quad (40)$$

$$\vec{S}=\begin{bmatrix} 0 \\ \frac{Gr}{Re^2}\theta g_\xi + S_E\, q\, E_\xi \\ \frac{Gr}{Re^2}\theta g_\eta + S_E\, q\, E_\eta \\ \frac{Gr}{Re^2}\theta g_\zeta + S_E\, q\, E_\zeta \\ \frac{S_E\ Ec}{c_{pe}'}\left[q(v+\frac{1}{RePr_E} E) - \frac{1}{Re\ D_E} \nabla q\right].E \\ 0 \end{bmatrix}$$

$$\mathbf{D} = \frac{1}{Re}\begin{bmatrix} 0 \\ \eta' \\ \eta' \\ \eta' \\ \frac{k'}{Pr\ c_{pe}'} \\ \frac{b'}{D_E} \end{bmatrix}^T \quad (41)$$

$$D\ 2(J\vec{Q}) = [\frac{D}{J} g_{ij} (J\vec{Q})_{,j}]_{,i} \quad (42)$$

where $J = \frac{\partial(\xi,\eta,\zeta)}{\partial(x,y,z)}$ is the determinant of the Jacobian geometric transformation matrix from physical x,y,z into computational ξ,η,ζ space, and g_{ij} is the metric tensor given by

$$g_{ij} = \nabla x_i' \nabla x_j' \tag{43}$$

Contravariant velocity components are related to velocity components in Cartesian coordinate system as follows

$$\begin{bmatrix} U \\ V \\ W \end{bmatrix} = \begin{bmatrix} \xi_x & \xi_y & \xi_z \\ \eta_x & \eta_y & \eta_z \\ \zeta_x & \zeta_y & \zeta_z \end{bmatrix} \begin{bmatrix} u \\ v \\ w \end{bmatrix} \tag{44}$$

The system (38) was solved using a four-stage Runge-Kutta explicit time stepping method[19]

$$\begin{aligned} \vec{Q}^0 &= \vec{Q}^n \\ \Delta \vec{Q}^m &= -\gamma_m \Delta t \ \vec{R}^{m-1} \quad m = 1,2,3,4 \\ \vec{Q}^{n+1} &= \vec{Q}^n + \Delta \vec{Q}^4 \end{aligned} \tag{45}$$

Here, the iteration level is denoted by n, and each stage of the Runge-Kutta method by m, where the coefficients are γ_m = 1/4, 1/3, 1/2 and 1, respectively. The residual $\vec{R}$ is defined as

$$\vec{R} = \frac{\partial \vec{E}}{\partial \xi} + \frac{\partial \vec{F}}{\partial \eta} + \frac{\partial \vec{G}}{\partial \zeta} - D^2(J\vec{Q}) - \vec{S} - \frac{\varepsilon_4 \psi}{8J\Delta t}\left[\frac{\partial^4}{\partial \xi^4} + \frac{\partial^4}{\partial \eta^4} + \frac{\partial^4}{\partial \zeta^4}\right](J\vec{Q}) \tag{46}$$

The last term in equation (46) represent fourth order artificial dissipation[19] which is added to improve the stability of the scheme and to prevent[16] the electric charge signs from changing locally in the flow field. The artificial dissipation sensor function, ψ, was based on a normalized value of the local gradient of the charge density distribution. The influence of artificial dissipation terms is controlled by ε_4 which are user-specified small parameters. Addition of fourth order artificial dissipation was found to be necessary in the simulation of the solidification processes only when the sharp gradients were created in velocity or in the charged particle density distribution.

To enhance the convergence rate, implicit residual smoothing was used when solving the Poisson's equation for the smoothed residual after each stage of the Runge-Kutta iteration.

$$\nabla^2 \hat{R}_i = \vec{R}^m{}_i \tag{47}$$

This equation was discretized and numerically solved by an alternate direction implicit scheme

$$(1 - \omega \delta_{\xi\xi})(1 - \omega \delta_{\eta\eta})(1 - \omega \delta_{\zeta\zeta}) \hat{R}_i = \vec{R}^m{}_i \tag{48}$$

where the smoothing operator is denoted by δ and ω is a user-specified constant, while $\hat{R}_i$ represents the smoothed residual. By introducing the artificial compressibility term in the continuity equation, the system of equations becomes hyperbolic. Therefore, boundary conditions have to be applied considering characteristic directions. Proper boundary conditions are determined from the nonconservative form of the transformed system. Wall boundary conditions for the pressure were computed from the normal momentum equation

$$\mathbf{n} \cdot \nabla \tilde{p} = \mathbf{n} \cdot \left[\frac{1}{Re} \nabla \cdot (\eta' \nabla \mathbf{v}) + \frac{Gr\ \theta}{Re^2} \mathbf{g} + S_E\, q\, \boldsymbol{E}\right] \tag{49}$$

Boundary conditions for electric charges on the vertical boundaries were of the Neumann type. The Poisson equation for the electric potential was solved separately during each global iteration using an ADI algorithm.

4. COMPUTATIONAL RESULTS

Mathematical and numerical models for solidification of a fluid flow were tested in the case of a rectangular two-dimensional container of aspect ratio 3:1. A uniform non-dimensional temperature θ = 1 was imposed at the bottom wall, a uniform cooling temperature θ = - 10 was enforced along the top wall and vertical walls were thermally insulated.

Gravitational force was acting vertically downward.

Two separate two-dimensional analysis computer codes were written that are based on the analytical formulation and the numerical algorithm summarized above. One code is capable of performing MHD solidification and the other code is capable of performing EHD solidification analysis. The container was filled with an electrically conducting fluid which was neutrally charged. It was discretized with 60 × 60 grid cells that were smoothly clustered towards the walls.

We have decided to simulate solidification of realistic melts used in electronics industry. Specifically, for MHD solidification we have used a silicon melt and for the examples of an EHD solidification we have used a gallium arsenide melt. The nondimensional numbers corresponding to the two melts are summarized in Table 1 and Table 2.

It should be pointed out that the value of the magnetic Prandtl number quoted in Table 1 is one order of magnitude larger than if the magnetic permeability for vacuum was used in the formula. This was done since the computer code tended to diverge when using the physical value for the magnetic Prandtl number. Identical problem was encountered when simulating solidification of blood flowing through a variable passage[10] subjected to an external magnetic field. In this case, the magnetic Prandtl number had to be increased ten orders of magnitude before a converging solution was obtained. Similarly, the electric Prandtl number quoted in Table 2 is approximately ten orders of magnitude larger than the actual physical value for the molten GaAs[23]. If smaller values for the electric Prandtl number were used, the EHD code with solidification tended to diverge rather quickly. The given cases represented a difficult task from a numerical point of view.

A CFL number of 2.8 corresponding to the maximum allowable value for the four step Runge-Kutta scheme was used together with a von Neumann number of the order 0.001. The value of the artificial compressibility parameter was $\beta = 10$ in all computer runs. In the explicit algorithm that we have used, the choice of β can affect[21] not only the convergence rate of the iterative process, but also the stability of the entire scheme. A more thorough linear stability analysis is definitely required of any iterative algorithm that is to be implemented in the MHD or the EHD solidification simulation.

We have occasionally used a small amount of fourth order artificial dissipation ($\varepsilon_4 = 0.005$) to allow for a smooth convergence. The results could be considered only as preliminary, because it was found[16] that even a very small amount of artificial dissipation necessary to enhance the convergence rate has a detrimental effect on the accurate prediction of the diffusion of charged particles.

4.1 MHD Computational Results

At first we were interested in learning about the silicon melt solidification involving no magnetic field and 100% of gravity. The computed velocity vector plot (Fig. 1a) indicate the existence of two recirculation zones, while the isotherms (Fig. 1b) indicate that the recirculation in this test case does not influence the solid/liquid interface shape.

Then, we repeated the test case with a uniform steady external magnetic field of 1 Tesla pointing downward as did 100% of gravity. Figure 2a indicates that the recirculation vortices have considerably weakened and migrated towards the side walls, while the predicted isotherms (Fig. 2b) demonstrate a deformation of the solid/liquid interface due to the presence of the magnetic field. A direct comparison of Figure1a and Figure 2a reveals that the amount of accrued solid phase is significantly lower in the case with the strong magnetic field.

In order to simulate a microgravity environment, the magnetic field was removed and the gravity field was reduced to 1%. The computed velocity vector plot (Fig. 3a) indicates a considerably weaker recirculation in the melt. It is interesting that the predicted amount of accrued solid and the corresponding isotherms (Fig. 3b) for this low-gravity test case are practically identical to the case with 100% gravity and no magnetic field.

From the convergence histories for these three runs (Fig. 4) it is evident that the solidification of silicon with a strong magnetic field proceeds at a significantly slower rate, while micro-gravity has a negligible effect on the solidification rate of this material.

4.2 EHD Computational Results

Since it is much easier to generate an electric potential field difference than it is to generate a strong magnetic field, it would be interesting to see what influence does an externally applied electric field have on a solidification process of GaAs. It was assumed that the rectangular container was initially filled with a GaAs melt. Initially, electrical charges were specified only at the injection boundary (lower wall). A steady external electric field was imposed by means of electrodes along the lower and the upper wall with an electric potential field difference of $\Delta\varphi$ = 100 V. Gravity force of 100% strength was applied vertically downward. The predicted electro-convective vortices were numerous and extremely strong in this case (Fig. 5a) causing irregularities in the melt/solid interface shape due to the strong micro vortices present there. Figure 5b depicts the predicted isotherms for this test case.

Next, the gravity force was reduced to 1% of its strength, while maintaining the electric potential difference as in the previous test case. The result was a significant reduction of the number and the strength of the vortices (Fig. 6a). The predicted isotherm plot (Fig. 6b) reveals that in the microgravity environment this test case achieved an improvement in the uniformity of the liquid/solid interface shape. The amount of accrued solid phase in both EHD cases was practically the same.

Finally, we changed the geometry of the container by making it a square. In this case the number of vortices (Fig. 7a), their strengths and locations were detremental to the smoothness of the solid/liquid interface (Figure 7b).

Conclusions

A separate magnetohydrodynamic and a separate electrohydrodynamic flow models including solidification have been developed. The models include Joule heating and latent heat release effects and Lorentz and ponderomotive forces. Gravity induced thermal buoyancy was incorporated via an extended Boussinesq approximation that allows for temperature dependent physical properties of the melt. It has been found that artificial dissipation causes excessive diffusion of charged particles and influences the convergence rate of the iterative process. Linear stability analysis of the existing numerical schemes need to be augmented to include the full MHD and EHD effects including solidification. Otherwise, the contemporary numerical iterative algorithms are highly unstable when attempting to perform computations with actual physical parameters for the solidifying melts. The existence of electro-convective vortices analogous to thermo-convective vortices has been computationally demonstrated and their significant weakening observed in the microgravity solidification simulation. This work is possible to extend into three dimensional separate MHD and EHD simulation packages as well as into a combined formulation for a joint MHD-EHD simulation which could include multiple charged species and physically unsteady magnetic and electric fields.

Results of these feasibility studies suggest possibilities for the development of an optimally controlled solidification process[24-25]. It should involve simultaneously variable thermal, magnetic and electric fields capable of achieving desired configurations of the solidifyed layers and desired distribution of different species within the layers.

Acknowledgments

We would like to expresses our gratitude to Mr. M. Long, Mr. R. Vermeland and Mr. K. Misegades of Cray Research, Inc. for donating computer time on their Cray-YMP and supporting the second author on a summer fellowship. Graphics were performed on computing equipment donated by Apple Computer, Inc.

References

1. Stuetzer, O. M., "Magnetohydrodynamics and Electrohydrodynamics," *The Physics of Fluids*, Vol. 5, No. 5, May 1962, pp. 534-544.
2. Landau, L. D. and Lifshitz, E. M., Electrodynamics of Continuous Media, Pergamon Press, New York, 1960.
3. Melcher, J. R., Continuum Electromechanics, The MIT Press, Cambridge, 1981.
4. Babskii, V. G., Zhukov, M. Y. and Yudovich, V. I., "Mathematical Theory of Electrophoresis," (translated by C. Flick), Consultants Bureau, New York, 1989.
5. Eringen, A. C., and Maugin, G. A., Electrodynamics of Continua I: Foundations

and Solid Media, Springer-Verlag, New York, 1990.

6. Eringen, A. C., and Maugin, G. A., Electrodynamics of Continua II: Fluids and Complex Media, Springer-Verlag, New York, 1990.
7. Lee, S. and Dulikravich, G. S., "Magnetohydrodynamic Flow Computations in Three Dimensions", AIAA Paper 91-0388, Reno, NV, Jan. 1991a; also in *International Journal for Numerical Methods in Fluids*, Vol. 13, No. 7, Oct. 1991, pp. 917-936.
8. Lee, S. and Dulikravich, G. S., "Computation of Magnetohydrodynamic Flow With Joule Heating and Buoyancy", Proceedings of International Aerospace Congress, Melbourne, Australia, May 13-17, 1991.
9. Dulikravich, G. S., Kosovic, B. and Lee, S., "Solidification of Variable Property Melts in Closed Containers: Magnetic Field Effects," Proc. 13th IMACS World Congress on Computation and Applied Math., Dublin, Ireland, July 22-26, 1991.
10. Kosovic, B., Dulikravich, G.S. and Lee, S., " Freezing Under the Influence of a Magnetic Field: Computer Simulation", Proc. 1991 ICHMT Internat. Symp. on Heat & Mass Transfer in Biomed. Eng., Editors: K. Diller, A. Shitzer, S. Seideman, Athens, Greece, Sept. 2-6, 1991.
11. Dulikravich, G. S., Kosovic, B. and Lee, S., "Solidification in Reduced Gravity With Magnetic Fields and Temperature-Dependent Physical Properties", ASME WAM'91, Atlanta, GA, Dec. 1-6, 1991, HTD-Vol. 175/MD-Vol.25, pp. 61-70, Heat and Mass Transfer in Solidification Processing, Editors: S.G. Advani and C. Beckermann.
12. Biscans, B., Hennequin, J. C., Bertrand, J., "Some Aspects of Continuous Flow Electrophoresis in Microgravity", *Acta Astronautica*, Vol. 13, No. 11/12, 1986, pp. 705-713.
13. Mazhorova, O. S., Popov, Y. P. Pokhilko, V. I. and Feonychev, A. I., "Numerical Investigation of Liquid Electrophoresis Without Support Media," Izvestia Academii Nauk SSSR, *Mekhanika Zhidkosti i Gaza*, No. 3, May-June 1988, pp. 14-20.
14. Bello, M. S. and Polezhaev, V. I., "Hydrodynamics, Gravitational Sensitivity and Transport Phenomena in Continuous Flow Electrophoresis," AIAA paper 91-0112, Aerospace Sciences Meeting, Reno, NV, Jan. 7-10, 1991.
15. Lee, S., Dulikravich, G. S.and Kosovic, B., "Computer Simulation of Electrophoretic Separation Processes," Proc. 17th Annual Northeast Bioeng. Conference, University of Connecticut, Hartford, CT, April 4-5, 1991.
16. Lee, S., Dulikravich, G.S. and Kosovic, B., "Electrohydrodynamic (EHD) Flow Modeling and Computations", AIAA paper 91-1469, AIAA Fluid Dynamics, Plasma Dynamics & Lasers Conf., Honolulu, HI, June 24-26, 1991.
17. Gray, D. D., and Giorgini, A., "The Validity of the Bousinessq Approximation for Liquids and Gases," *International Journal of Heat and Mass Transfer*, Vol. 19, 1976, pp. 545-551.
18. Poirier, D. and Salcudean, M., "On Numerical Methods Used in Mathematical Modeling of Phase Change in Liquid Metals", ASME paper 86-WAM/HT-22, Anaheim, CA, Dec. 7-12, 1986.
19. Jameson, A., Schmidt, W., and Turkel, E., "Numerical Solutions of the Euler Equations by Finite Volume Methods Using Runge-Kutta Time-Stepping Scheme," AIAA paper 81-1259, Palo Alto, CA, June, 1981.
20. Chorin, A. J., "A Numerical Method for Solving Incompressible Viscous Flow Problems," *Journal of Computational Physics*, Vol. 2, 1967, pp. 12-26.
21. Lee, S. and Dulikravich, G.S., "Performance Analysis of DMR Method for Acceleration of Iterative Algorithms", AIAA paper 91-0241, Reno, NV, Jan. 7-10, 1991.
23. Brodsky, M. H., "Properties of Gallium Arsenide", 2nd edition, INSPEC, EMIS Datareview Series No. 2, 1990.
24. Ivory, C. F., Gobie, W. A., Bekwith, J. B., Hergenrother, R. and Malec, M., "Electromagnetic Stabilization of Weakly Conducting Fluids", *Science*, Vol. 238, Oct. 1987, pp. 58-61.
25. Dulikravich, G.S. and Hayes, L. J., "Control of Surface Temperatures to Optimize Survival in Cryopreservation", ASME WAM'88, Chicago, IL, Nov. 27-Dec. 2, 1988, Symp. on Comput. Meth. in Bioeng., Editors: R. L. Spilker and B.R. Simon, BED-Vol. 9, pp. 255-265.

Re	8300
Gr	56.769×10^6
Ec	7.869×10^{-8}
Pr	0.0116
Fr	0.071392
Pr_m	4.44×10^{-6}
H\s\do3	$2093B_o$

Table 1. Input parameters for MHD solidification of silicon melt in a 3:1 container with 100% gravity

$\Delta\varphi$(V)	100
Re	87.6
Gr	7683.
Ec	5.7610^{-8}
Pr	0.068
S_e	0.007
D_e	10^{-10}
Pr_e	1.
N_e	8.556

Table 2. Input parameters for EHD solidification of GaAs melt in a 3:1 container with 100% gravity

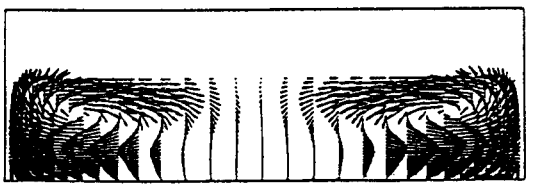

Figure 1a. Silicon solidification without MHD; velocity vector field for 100% gravity case

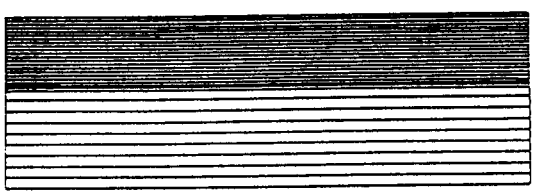

Figure 1b. Silicon solidification without MHD; isotherms for 100% gravity case

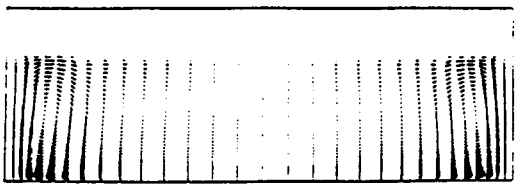

Figure 2a. Silicon solidification with MHD; velocity vector field for 100% gravity case

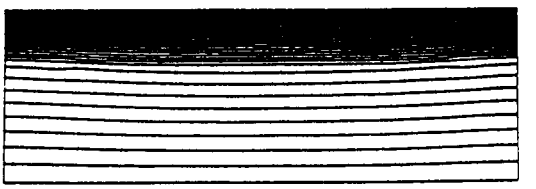

Figure 2b. Silicon solidification with MHD; isotherms for 100% gravity case

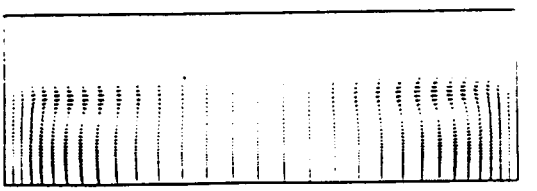

Figure 3a. Silicon solidification without MHD; velocity vector field for 1% gravity case

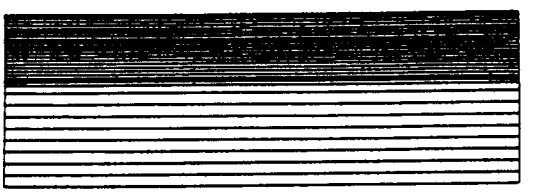

Figure 3b. Silicon solidification without MHD; isotherms for 1% gravity case

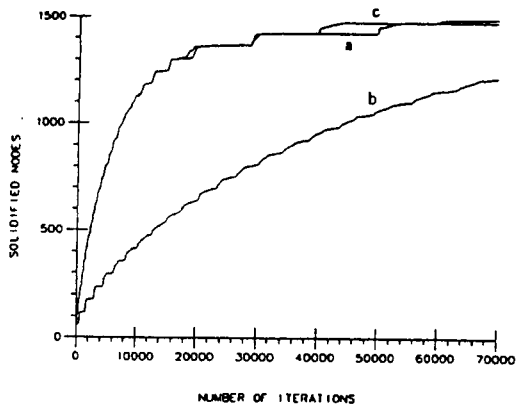

Figure 4. Silicon solidification: number of solidified cells for the three cases: a) no MHD with 100% gravity; b) MHD with 100% gravity; c) no MHD with 1% gravity.

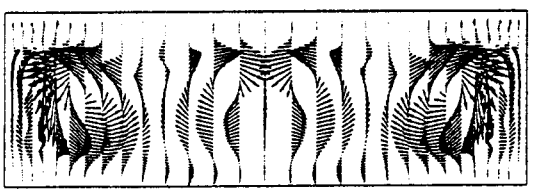

Figure 5a. GaAs solidification with EHD; velocity vector field for 100% gravity case

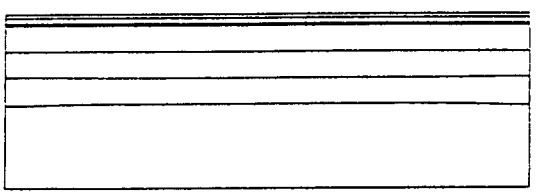

Figure 5b. GaAs solidification with EHD; isotherms for 100% gravity case

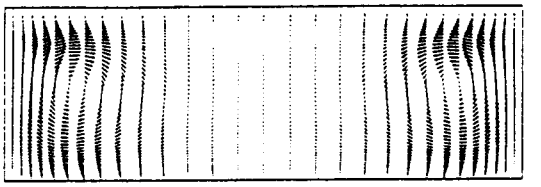

Figure 6a. GaAs solidification with EHD ; velocity vector field for 1% gravity case

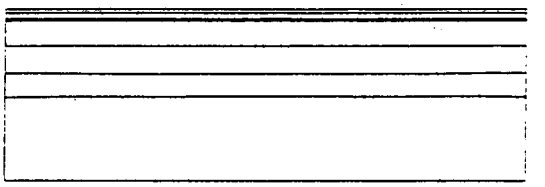

Figure 6b. GaAs solidification with EHD ; isotherms for 1% gravity case

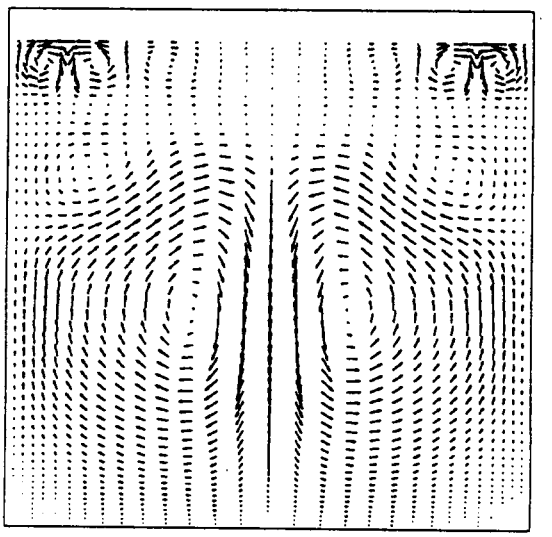

Figure 7a. GaAs solidification with EHD; velocity vector field for 100% gravity case. Square cavity.

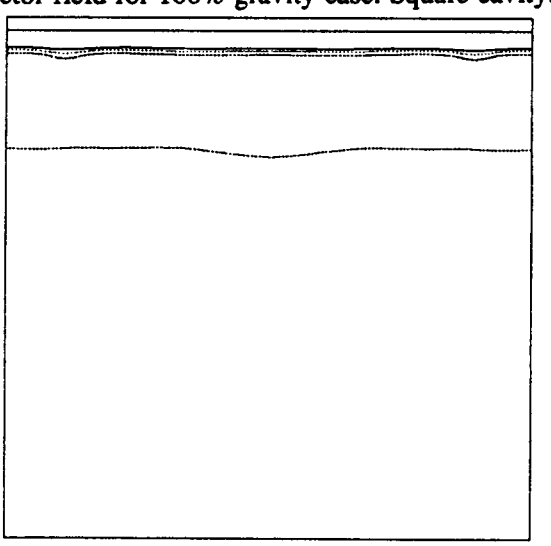

Figure 7b. GaAs solidification with EHD; isotherms for 100% gravity case. Square cavity.